

BRAIN COMMUNICATIONS

Structural brain networks and functional motor outcome after stroke—a prospective cohort study

Eckhard Schlemm,¹ Robert Schulz,¹ Marlene Bönstrup,^{1,2} Lutz Krawinkel,¹ Jens Fiehler,³ Christian Gerloff,¹ Götz Thomalla¹ and Bastian Cheng¹

The time course of topological reorganization that occurs in the structural connectome after an ischaemic stroke is currently not well understood. We aimed to determine the evolution of structural brain networks in stroke patients with motor deficits and relate changes in their global topology to residual symptom burden and functional impairment. In this prospective cohort study, ischaemic stroke patients with supratentorial infarcts and motor symptoms were assessed longitudinally by advanced diffusion MRI and detailed clinical testing of upper extremity motor function at four time points from the acute to the chronic stage. For each time point, structural connectomes were reconstructed, and whole-hemisphere global network topology was quantified in terms of integration and segregation parameters. Using non-linear joint mixed-effects regression modelling, network evolution was related to lesion volume and clinical outcome. Thirty patients were included for analysis. Graph-theoretical analysis demonstrated that, over time, brain networks became less integrated and more segregated with decreasing global efficiency and increasing modularity. Changes occurred in both stroke and intact hemispheres and, in the latter, were positively associated with lesion volume. Greater change in topology was associated with larger residual symptom burden and greater motor impairment 1, 3 and 12 months after stroke. After ischaemic stroke, brain networks underwent characteristic changes in both ipsi- and contralesional hemispheres. Topological network changes reflect the severity of damage to the structural network and are associated with functional outcome beyond the impact of lesion volume.

1 Klinik und Poliklinik für Neurologie, Kopf- und Neurozentrum, Universitätsklinikum Hamburg-Eppendorf, 20246 Hamburg, Germany

2 Klinik und Poliklinik für Neurologie, Universitätsklinikum Leipzig, Leipzig, Germany

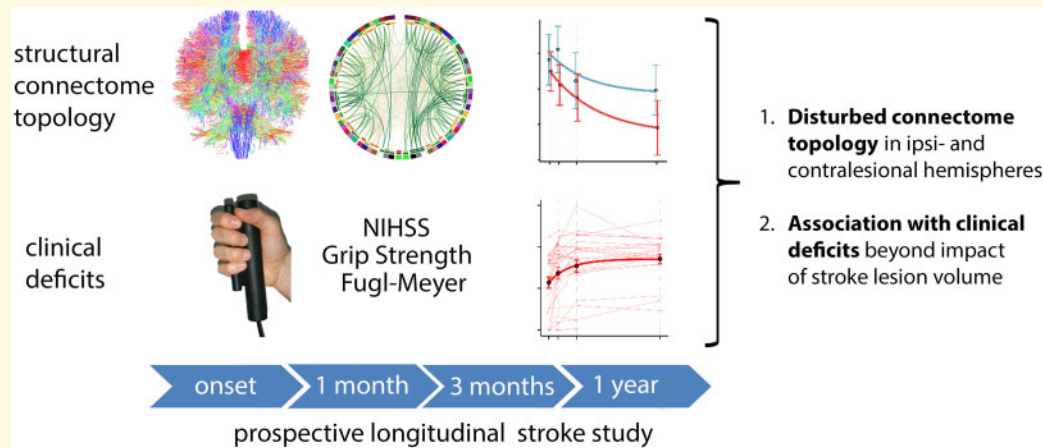
3 Klinik und Poliklinik für Neuroradiologische Diagnostik und Intervention, Universitätsklinikum Hamburg-Eppendorf, Hamburg, Germany

Correspondence to: Eckhard Schlemm, MBBS, PhD Klinik und Poliklinik für Neurologie Kopf- und Neurozentrum, Universitätsklinikum Hamburg-Eppendorf, Martinistraße 52, 20246 Hamburg, Germany
E-mail: e.schlemm@uke.de

Keywords: graph theory; ischaemic stroke; motor function; recovery; structural connectivity

Abbreviations: AIC = Akaike information criterion; d = days; DTI = diffusion-tensor imaging; FM = Fugl-Meyer; ICH = intracerebral haemorrhage; IQR = inter-quartile range; m = months; MCA = middle cerebral artery; NIHSS = National Institutes of Health Stroke Scale; q_{50} = median connectivity; rGS = relative grip strength; ROI = region of interest; SAH = subarachnoid haemorrhage; SE = standard error

Graphical Abstract



Introduction

With over 50 million years of healthy life lost each year due to stroke-related death and disability, brain infarcts contribute significantly to the burden of disease worldwide (Bill and Foundation, 2019). Ischaemic lesions affect neurological functions, such as motor execution and control, vision, cognition and speech, as well as functional independence. These deficits result not only from focal damage to cortical areas and white matter tracts at the site of ischaemia, but also from secondary effects on structural integrity in remote brain areas that are directly or indirectly synaptically linked to the primary lesion (Seitz et al., 1999; Carrera and Tononi, 2014, Cheng et al., 2014b).

A growing body of evidence suggests that normal neurological function does not only depend on the structural and functional integrity of specific grey and white matter regions of the brain but is instead contingent on the balanced interplay of activity in multiple interconnected populations of neurons (Griffa et al., 2013; Fornito and Bullmore, 2015). The structural connectome represents fibre tracts connecting pairs of cortical areas and forms the structural basis for this large-scale tempo-spatial organization (Sporns, 2013). In order to support both segregation between groups of functionally specialized brain areas and long-range integration of remote processing units, connections in the structural connectome are arranged in a small-world configuration, balancing these two opposing organizational principles (Watts and Strogatz, 1998; Hilgetag et al., 2000; Sporns and Honey, 2006; Achard and Bullmore, 2007). In the growing field of network science, the topological notions of segregation and integration have been operationalized in the form of graph-theoretical measures, such as modularity and efficiency (Bullmore and Sporns, 2009). Changes in the structural brain network have been implicated in a variety of conditions such as epilepsy

(Lemkaddem et al., 2014, Gleichgerrcht et al., 2015a), schizophrenia (Fornito et al., 2012; Van Den Heuvel and Fornito, 2014), small vessel disease (Lawrence et al., 2014; Xu et al., 2018), dementia (Tuladhar et al., 2016; Lawrence et al., 2018), migraine (Liu et al., 2012), multiple sclerosis (Kuceyeski et al., 2018) and Tourette's syndrome (Cheng et al., 2014a; Schlemm et al., 2017).

Analysis of structural connectivity has proved particularly useful in ischaemic stroke patients as a tool to assess non-local changes in brain architecture (Carrera and Tononi, 2014, Cheng et al., 2019b); as an intermediate phenotype between the focal lesion and observed clinical deficits (Lim and Kang, 2015); as well as a marker for recovery potential following the acute phase (Koch et al., 2016). In addition to alterations in the functional connectome of stroke patients as studied by EEG and functional MRI, there is also evidence for disrupted structural topology in the chronic phase after stroke. The integrity of specific cortico-cortical connections such as ipsilesional parietofrontal pathways (Schulz et al., 2015), the superior longitudinal fascicle (Schaechter et al., 2009), transcallosal (Wang et al., 2012) and dorsal premotor-primary motor connections (Schulz et al., 2017), are all related to residual motor function. At the global network level, taking into account the integration and segregation of all brain regions within the structural connectome, it was found that network communicability, a marker for the ease of information transfer, was reduced around the stroke lesion (Crofts et al., 2011). However, the progression of structural changes, in particular, the evolution of topological properties of the structural connectome with time after stroke and its relation to the clinical course is less well understood.

Therefore, in this longitudinal cohort study, we reconstructed structural connectomes of stroke patients with motor symptoms in the upper limb, aiming to relate changes in their global topology to clinical outcome. At four time points covering the acute, subacute and chronic

phases after stroke, we used probabilistic fibre tracking to reconstruct whole-brain structural connectomes from diffusion-weighted imaging and employed graph theory to quantify aspects of their global topology. We specifically investigated changes in the ipsi- and contralesional hemispheres and hypothesized that focal stroke lesions induce alterations in the structural connectome of stroke patients, disrupting the balance between integration and segregation required for normal neurological function. Region-specific topological parameters were calculated to localize global disruptions to distinct parts of the brain network. We expected that the magnitude of topological alterations would be associated with the extent of the ischaemic lesion and related to clinical deficits in motor function.

Materials and methods

Study design

Patients with acute ischaemic stroke admitted to our Stroke Unit at the Universitätsklinikum Hamburg-Eppendorf were screened between June 2012 and September 2017 to form the Collaborative Research Centre (CRC) 936 stroke cohort. Inclusion criterion for the present study was a first-ever supratentorial ischaemic stroke (as demonstrated by MRI) with an upper extremity motor deficit. Exclusion criteria were significant cognitive symptoms like aphasia or hemianopia, or cognitive impairment rendering the patient incapable to give informed consent or comply with instructions for clinical testing. Also, patients with contraindications to MRI as well as the presence of marked white matter lesions, intracerebral haemorrhage or evidence of pre-existing structural brain lesions were excluded. Patients with imaging data of insufficient quality; or with extensive cortical infarcts hindering image registration and automated cortical segmentations; or with imaging data from fewer than two time points, were excluded from the analysis. After providing written informed consent according to the Declaration of Helsinki, patients underwent cerebral imaging and clinical testing of motor function at baseline in the acute phase (3–5 days post-stroke), as well as in the subacute and chronic phases 30–40, 85–95 and 340–380 days after stroke. The study was approved by the ethics committee of the chamber of physicians Hamburg, Germany (PV 37777).

Clinical testing

At each of the four time points, global stroke severity was assessed using the National Institutes of Health Stroke Scale (NIHSS) (Lyden, 2017). Motor function in the affected hand was operationalized as whole-hand grip strength relative to grip strength in the unaffected hand (rGS). Absolute grip strength in each hand was obtained

from averaging three consecutive measurements using the Strength JAMAR hand evaluation kit (Elite healthcare, UK). Active movement range and synergies of proximal and distal muscles were further quantified on the ordinal upper extremity Fugl-Meyer (FM) scale (Fugl-Meyer *et al.*, 1975).

Imaging

We acquired imaging data on a 3T Siemens Skyra MRI scanner (Siemens, Erlangen, Germany). A 32-channel head coil was used to measure both diffusion-weighted and high-resolution T1-weighted anatomical images. For diffusion-weighted imaging, 75 axial slices were obtained covering the whole brain with gradients ($b = 1500 \text{ s/mm}^2$) applied along 64 non-collinear directions with the sequence parameters: repetition time (TR) = 10 000 ms, echo time (TE) = 82 ms, field of view (FOV) = 256×204 , slice thickness (ST) = 2 mm and in-plane resolution (IPR) = $2 \times 2 \text{ mm}^2$. The complete dataset consisted of $2 \times 64 b_{1500}$ images and additionally one b_0 image at the beginning and one after the first 64 images. For anatomical imaging, a 3D magnetization-prepared, rapid acquisition gradient-echo sequence (MPRAGE) was used with the following parameters: TR = 2500 ms, TE = 2.12 ms, FOV = $240 \times 192 \text{ mm}^2$, 256 axial slices, ST = 0.94 mm and IPR = $0.94 \times 0.94 \text{ mm}^2$. In addition, fluid-attenuated inversion recovery sequences were acquired in the acute phase 3–5 days after stroke for delineation of ischaemic lesions (TR = 9000 ms, TE = 90 ms, TI = 2500 ms, FOV = $230 \times 230 \text{ mm}^2$, ST = 5 mm and IPR = $0.7 \times 0.7 \text{ mm}^2$).

Network construction

Undirected, weighted networks were constructed based on high-resolution structural imaging, diffusion-tensor imaging and probabilistic tractography to approximate white matter fibre tracts as described previously (Schlemm *et al.*, 2017). In summary, diffusion-weighted images were analysed using the FSL software package 5.1 (<http://www.fmrib.ox.ac.uk/fsl>). All datasets were corrected for eddy currents and head motion. Structural T1-weighted anatomical images were processed using the FreeSurfer software package 5.3.0 with standard procedures and parameters resulting in a parcellation of the cerebral grey matter into 33 cortical and 3 subcortical regions per hemisphere (Desikan *et al.*, 2006; Behrens *et al.*, 2007). For cortical regions, masks from automated parcellation by FreeSurfer were refined to delineate the grey–white matter boundary underlying the cortical areas to increase anatomical accuracy for DTI fibre tracking. Therefore, surface maps of the boundary between grey and white matter were generated by FreeSurfer and applied to constrain parcellation masks to a ribbon directly underlying the cortical grey matter. All resulting masks were visually checked for plausibility and accuracy. In total,

72 masks (36 per hemisphere) were created as listed in [Supplementary Table 1](#). Processing of diffusion data included application of a probabilistic diffusion model modified to allow estimation of multiple ($n=2$) fibre directions using the program bedpostX. From each seed ROI voxel, 5000 streamlines were initiated through the probability distribution of principle fibre directions. Structural connectivity between two regions was measured by masking the results of each seed ROI by each of the remaining ROIs. Weighted connectivity matrices were computed by defining the strength of the connection from ROI s to ROI t as the raw number of streamlines starting in s and running through t , divided by the sum of the volumes of s and t ([Hagmann et al., 2008](#)). Network reconstruction resulted in whole-brain connectivity matrices of dimension 72×72 , which were symmetrized by averaging with their own transpose. Intra-hemispheric networks were defined as induced subgraphs, corresponding to the upper and lower diagonal blocks of the whole-brain connectivity matrix. Lesion volumes were measured on fluid-attenuated inversion recovery data at the first time point, 3–5 days after stroke, as described previously ([Cheng et al., 2015](#)). The density of a network was defined as the proportion of theoretically possible connections with a positive weight.

Graph theory

The median edge weight q_{50} was calculated as a numerical measure of global connectivity for each intra-hemispheric network. Subsequently, topological properties of individual connectomes were summarized by the commonly used global graph parameters ‘efficiency’ as a measure of integration, and ‘modularity’ as a measure of segregation ([Bassett and Bullmore, 2009](#)). Global efficiency is defined as the average inverse shortest path length in the network, modularity quantifies the extent to which a network can be partitioned into non-overlapping, relatively weakly interconnected sub-networks. These measures are known to reflect important organizational principles of the brain connectome ([Bertolero et al., 2015](#)) and are sensitive to detecting structural and functional network changes in a variety of neurological disorders ([Singh et al., 2013](#); [Ajilore et al., 2014](#); [Tuladhar et al., 2016](#)), including ischaemic stroke ([Yang et al., 2015](#); [Siegel et al., 2016, 2018](#)). For the main analysis, graph parameters were computed for dense weighted connectomes without thresholding ([Civier et al., 2019](#)). The effect of removing a proportion of weak connections to enforce lower network densities ranging from 10% to 90% was explored in a sensitivity analysis ([Buchanan et al., 2019](#)).

Local connectivity in the networks was summarized by computing, for each node, the sum of the weights of the incident connections (strength), as well as the efficiency of the sub-network induced by itself and its neighbours, and local clustering ([Rubinov and Sporns, 2010](#)). All

graph-theoretical computations were performed in the Brain Connectivity Toolbox for Matlab ([Rubinov and Sporns, 2010](#)).

Statistical analysis

Numerical processing of network matrices and calculation of graph measures was carried out in Matlab version R2017a ([The MathWorks, 2017](#)). All statistical analyses were performed in the R language for statistical computing, R version 3.5.3 beta ([R Core Team, 2019](#)). P -values in the main text are reported unadjusted as a continuous measure of strength of evidence with values less than 0.05 occasionally, and in agreement with common practice, referred to as statistically significant. However, given the lack of a pre-registered analysis protocol, no formal statistical tests were carried out in this study. Where applicable in the case of mass-univariate multiple testing, Bonferroni corrections were used to aid interpretation of our results. No imputation for missing data was performed.

Clinical data

Lesion volume was transformed logarithmically and analysed for differences between left- and right-hemispheric infarcts using a two-sample t -test. Clinical outcome measures of symptom burden (NIHSS score) and motor impairment (relative grip strength, FM score) at each of four time points between the acute (3–5 days after stroke) and chronic (1 year after stroke) phases were assessed for association with side and volume of the lesion, as well as age and sex of the patient. Simple linear regressions were used for grip strength. Poisson regressions with a logarithmic link were used to model NIHSS and FM scores as approximate count data; in the presence of over-dispersion conditional variances were modelled as linear functions of the conditional means ([Ver Hoef and Boveng, 2007](#)).

It is known that recovery of motor function after ischaemic stroke follows a non-linear trajectory with the largest improvement occurring until 3–6 months post-stroke and only marginal further gain in motor function after 6 months ([Kelly-Hayes et al., 1989](#); [Nakayama et al., 1994](#); [Jørgensen et al., 1995](#); [Hendricks et al., 2002](#); [Verheyden et al., 2008](#)). After visual inspection of the evolution of outcome parameters in our patients ([Fig. 1](#)), the course of clinical improvement was, therefore, modelled by exponential functions of time as done previously ([Abela et al., 2012](#)) and compared with linear models using the Akaike information criterion (AIC) ([Akaike, 1974](#)). In the model equation,

$$\text{Outcome}_t \sim a + \Delta(1 - e^{-b t}), \quad (1)$$

$$t \in \{3 - 5 \text{ days}, 1, 3 \text{ and } 12 \text{ months}\},$$

the parameter a can be identified as the initial severity of symptoms; Δ is the difference in outcome between the

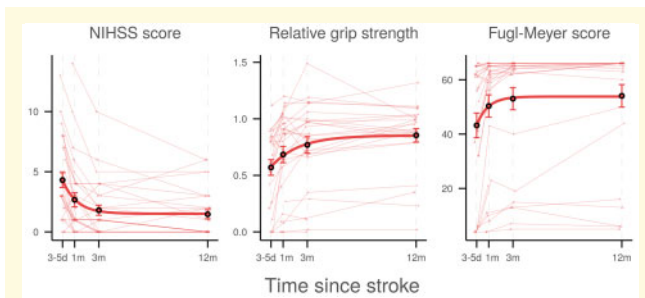


Figure 1 Temporal profiles of clinical outcome parameters. Horizontal axes indicate time after stroke. Thin lines represent linearly interpolated profiles for individual patients. Diamonds and triangles indicate patients with left- and right-sided lesions, respectively. Circles and bars denote cross-sectional means and asymptotic standard errors, respectively. Thick lines visualize the non-linear model, $Outcome_t \sim a + \Delta(1 - \exp(-b t))$. d = days; m = months; NIHSS = National Institutes of Health Stroke Scale.

acute and late chronic phase; and b represents a nuisance parameter that can be interpreted as the rate of recovery. The model included a random subject-specific intercept to account for the longitudinal design of the study and was fit using non-linear mixed-effects regression (Pinheiro *et al.*, 2019). Residuals were assumed to be normally distributed and uncorrelated both within and between subjects.

Structural network properties

In a first step, the effect of time on numerical global intra-hemispheric connectivity was modelled via both linear and exponential functions. Models were compared using the AIC. In the exponential model, differences in the time course between stroke and intact hemispheres were examined by allowing the model parameters a and Δ to vary according to whether or not the hemisphere was containing the stroke lesion (ipsilesional or contralesional hemisphere, subsequently referred to as ‘hemisphere condition’). Statistical significance was assessed using t -tests as implemented in the nlme package for R (Pinheiro *et al.*, 2019). Time courses in stroke and intact hemispheres were then quantified separately by performing individual exponential growth curve analyses.

Similarly, the time courses of the global graph parameters efficiency and modularity after stroke were modelled non-linearly as exponential functions of time. The interaction between time and hemisphere condition was accounted for as above via hemisphere-condition-dependent model parameters.

The effect of time on local network architecture was investigated by a mass-univariate non-linear regression analysis of strength, local efficiency and local clustering of individual nodes in the connectome. Brain regions with an accelerated decline of local network integrity were identified by a statistically significant effect of

hemisphere condition on the model parameter Δ in a mixed-effects exponential regression analysis as before.

Relation of network properties to lesion volume

After quantifying the time course of numerical connectivity as well as global and local network topology and assessing differences between ipsi- and contralesional hemispheres, we investigated the effect of lesion volume on patterns of post-stroke changes in the structural connectome. To this end, exponential mixed-effects regressions using the R function nlme were performed, including the logarithm of lesion volume as an additional linear predictor for the total structural network change between acute and chronic phase (model parameter Δ).

Relation of network properties to clinical outcome measures

We hypothesized that changes in structural brain network architecture are associated with clinical outcome. In principle, simple linear and quasi-Poisson regressions were used to assess the relation between change in numerical connectivity, global graph measures and clinical parameters 1, 3 and 12 months after stroke. Specifically, observations from these time points were pooled using a two-stage approach (Laird and Ware, 1982; Zhang *et al.*, 2007). First, a mixed-effects regression with subject-specific random intercept was performed to estimate the effect of time on structural network change. In a second step, NIHSS values and motor function scores (relative grip strength and upper extremity FM) were regressed against subject-specific predicted network change from the first step at each time point. The effect of lesion volume as a potential confounder was examined by including it as a nuisance regressor at the second stage. This two-step method takes into account the relationship between serial observations on the same subject as well as the time-varying nature of both clinical outcome and network topology. At the same time, it obviates the need for a computationally intensive joint modelling of predictor and response in a Bayesian setting (Rizopoulos, 2012; Sayers *et al.*, 2017). For adequate comparison, we also examined associations between absolute value of global network properties and clinical outcome.

Data availability

Clinical data and global graph measures analysed in this study are included in [Supplementary Appendix A](#) and as a separate CSV file. Further data, including code used for the analyses, are available upon reasonable request from the corresponding author.

Results

Forty-eight patients were considered for inclusion in the study. At the end of the recruitment period, 18 patients

were excluded from the analysis for reasons detailed in [Supplementary Fig. 1](#). In summary, 1 patient demonstrated extensive stroke lesions preventing reliable registration and automated cortical segmentations and 17 patients were lost to follow-up. In total, clinical and imaging data from the remaining 30 patients as detailed in [Supplementary Table 2](#) were included in the analysis.

Imaging and clinical testing in the acute phase took place after a median of 4 [inter-quartile range (IQR) 3–5] days. Assessment in the early to late subacute and chronic phases was performed 5.0 (4.3–6.1), 14.5 (13.3–16.0) and 51.9 (49.3–53.4) weeks after stroke, respectively.

Clinical data

Baseline demographics

Of the 30 stroke patients included for analysis, 12 were female; age was 64.7 ± 12.5 years (mean \pm standard deviation); 16 (53.3%, CI_{95} [34.6, 71.2]%) had a lesion in the left hemisphere; the infarct volume as measured at the first time point, 3–5 days after stroke, ranged from 0.6 to 69.2 ml (median 3.4 ml, IQR 1.7–16.5 ml). The lesions were predominantly located in subcortical brain areas, involving the centrum ovale, the corona radiata and the internal capsule ([Supplementary Fig. 2](#)). Lesions in the left and right hemispheres were of comparable size ($P=0.27$).

Initial severity of stroke symptoms ranged from 0 to 13 on the NIH Stroke Scale (median 3, IQR 2–7). In this group of clinically mildly to moderately affected patients, quasi-Poisson regressions indicated that patients with larger infarct volumes were affected more severely in the acute phase ($P_{3-5d} = 0.04$), but not at the later time points at 1, 3 or 12 months after stroke. There was no effect of side of the lesion, nor age or sex of the patient, on stroke severity.

Impairments in motor function and residual function of the affected hand were quantified in the acute phase as relative grip strength ranging from 0 to 1.12 (median 0.68, IQR 0.26–0.83) and FM score ranging from 4 to 66 (median 56, IQR 32–63). In these motor specific outcome measures, there was no statistically significant association with infarct size or side of the lesion, nor with age or sex of the patient.

Given these baseline results, and to increase the parsimony of our models, side of the lesion, age and sex of the patient were not included as covariates in subsequent non-linear regression analyses.

Time course of symptom severity and motor function

Over the observation period, most patients improved clinically as demonstrated in [Fig. 1](#). Frequently, no relevant clinical deficits were observed 1 year after stroke: The median NIHSS score improved to 0 (IQR 0–2.25), median ratio of grip strength to 0.91 (IQR 0.82–1.02) and median FM score to 66 (IQR 57.5–66). Growth curve

Table 1 Statistical details of clinical time course

Clinical outcome		Point estimate	SE	P
NIHSS	a	4.552	0.520	1.75e-13
	b	1.199	0.341	7.00e-04
	Δ	-3.033	0.320	6.03e-15
rGS	a	0.482	0.072	3.26e-09
	b	1.040	0.333	2.52e-03
	Δ	0.288	0.036	8.71e-12
FM	a	41.690	4.224	1.06e-15
	b	5.093	21.090	8.10e-01
	Δ	10.860	1.430	3.98e-11

Point estimates, standard errors and P -values for model parameters a (initial value), b (rate of change) and Δ (total amount of change) obtained from fitting the exponential model (1) to temporal profiles of clinical outcome parameters. Standard errors and P -values result from non-linear mixed-effects regressions fit using the R package nlme. P -values for Δ of less than 0.05 are marked in bold.

FM = Fugl-Meyer; NIHSS = National Institutes of Health Stroke Scale; rGS = relative grip strength; SE = standard error.

analyses indicated statistical superiority of exponential models ($AIC_{exp}^{NIHSS} = 490.2$, $AIC_{exp}^{rGS} = -17.2$, $AIC_{exp}^{FM} = 877.2$) over linear fits ($AIC_{lin}^{NIHSS} = 524.2$, $AIC_{lin}^{rGS} = 10.7$, $AIC_{lin}^{FM} = 905.2$) for the time course of each of the three outcome variables ([Table 1](#)).

Network properties

The mean intra-hemispheric network density, i.e. the proportion of non-zero connections, was $95.7\% \pm 1.6\%$ with no significant differences between ipsi- and contralesional hemispheres or between time points.

Effects of time and hemisphere condition on global graph measures

During the acute stage, 3–5 days after stroke, no differences in median edge weight q_{50} or topological graph measures were observed between ipsi- and contralesional hemispheres. Analysis of numerical measures of intra-hemispheric connectivity revealed that, based on the AIC, the time course of q_{50} was better described by an exponential than a linear model ($AIC_{exp} = -1038.3$, $AIC_{lin} = -992.2$). The temporal profiles of intra-hemispheric q_{50} ([Fig. 2](#)) did not differ significantly between ipsi- and contralesional hemispheres with a trend towards larger decline in stroke hemispheres ($\Delta_{ipsi} = -0.0060 \pm 0.0038$, $P=0.11$). Subgroup modelling showed a significant exponential decline of median edge weight in stroke hemispheres ($\Delta = -0.0076 \pm 0.0037$, $P=0.04$; $AIC_{exp} = -544.1$, $AIC_{lin} = -523.0$), but did not reveal a significant effect of time on q_{50} in contralesional hemispheres ($\Delta = -0.0038 \pm 0.0045$, $P=0.39$; $AIC_{exp} = -509.2$, $AIC_{lin} = -486.7$). Further details, including estimates of the nuisance model parameters a and b are given in [Supplementary Table 3](#).

Growth curve analysis of whole-hemisphere global graph parameters using non-linear mixed-effects regression modelling revealed consistent effects of time ([Fig. 2](#), [Table 2](#)). Global efficiency declined exponentially over

time in the ipsilesional hemisphere but not the contralesional hemispheres. Modularity increased significantly in both hemispheres, with a numerically larger effect ipsilesionally. These effects were not sensitive to the choice of network density and persisted over a wide range of thresholds (Supplementary Figs 3 and 4). Inclusion of age and sex as nuisance regressors did not substantially change the results (not shown).

As detailed in the Supplementary Tables 4 and 5, changes in the local graph parameters strength, efficiency and clustering were larger in ipsilesional than contralesional hemispheres, and most pronounced in parts of the frontal, parietal and limbic lobes involving primary motor, premotor and supplementary motor areas as well as the cingulate cortex.

Association of network properties with lesion volume

Global network measures at different time points after stroke are depicted in relation to lesion volume in Fig. 3.

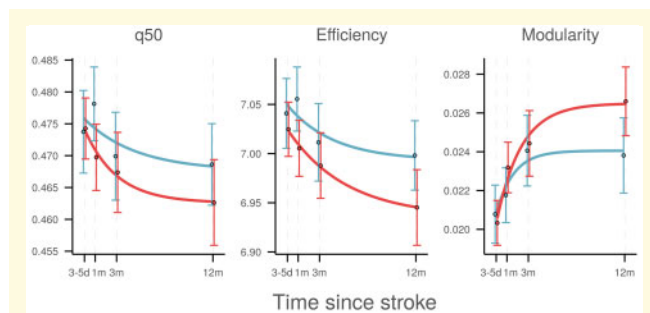


Figure 2 Time course of global graph measures. Temporal profile of intra-hemispheric global network measures in ipsilesional (red) and contralesional (blue) hemispheres. Horizontal axes indicate time after stroke. Circles and bars represent cross-sectional means and standard errors, respectively. Solid lines visualize modelled exponential change. d = days; m = months; q_{50} = median connectivity.

Non-linear mixed-effects modelling revealed a significant positive association between lesion volume and global connectivity decline in ipsilesional but not contralesional hemispheres ($P_{\text{interaction}} = 4.90 \times 10^{-5}$). Specifically, greater loss of ipsilesional median connectivity was observed in patients with larger stroke lesions. Analogous effects were observed for markers of global network topology with higher lesion volumes being associated with a larger decline in ipsilesional efficiency and larger increase in ipsilesional modularity. There was no evidence of a relationship between size of the infarct and contralesional network metrics. Statistical details are provided in Table 3. These effects were stable across network densities imposed by proportional thresholding of network matrices (Supplementary Figs 5 and 6). Paralleling global topology, change in local network integrity on the side of the lesion, but not contralesionally, was modulated by lesion volume (Supplementary Tables 6 and 7).

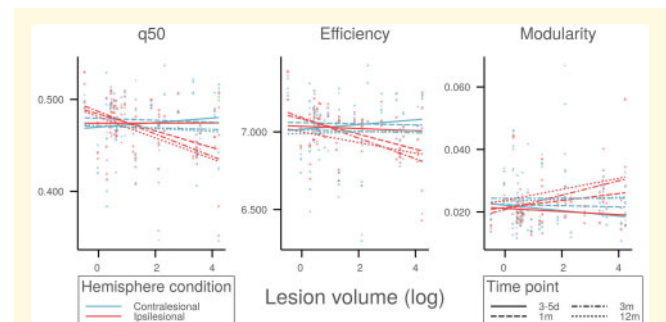


Figure 3 Association between global topology and infarct size. Relation between global network measures of ipsilesional (red) and contralesional (blue) hemispheres, and stroke lesion volume. Line segments represent cross-sectional predicted means of network measures in the acute (3–5 days, squares, solid), subacute (1 month, circles, dashed; 3 months, triangles, dot-dashed), and chronic (12 months, diamonds, dotted) phases after stroke. q_{50} = median connectivity.

Table 2 Statistical details of time course of global graph measures

		Joint model			Ipsilesional			Contralesional		
		Estimate	SE	P	Estimate	SE	P	Estimate	SE	P
Efficiency	a	7.024	0.030	1.29e-238	7.008	0.032	3.82e-114	7.039	0.035	4.97e-111
	b	1.094	1.114	0.3272	1.092	1.072	0.3117	1.096	1.913	0.5683
	Δ	-0.017	0.021	0.4101	-0.050	0.019	0.0110	-0.031	0.021	0.1465
	Δ_{ipsi}	-0.047	0.020	0.0215						
Modularity	a	0.021	0.001	1.64e-34	0.021	0.002	1.11e-23	0.021	0.002	1.13e-20
	b	0.997	0.595	0.0952	0.996	0.536	0.0668	0.998	0.956	0.2994
	Δ	0.003	0.001	0.0045	0.005	0.001	1.04e-05	0.003	0.001	0.0098
	Δ_{ipsi}	0.002	0.001	0.0663						

Point estimates, standard errors and *P*-values of model parameters obtained from fitting the exponential model (1) to temporal profiles of intra-hemispheric global graph parameters. In the joint model, the parameter of topological change, Δ , was allowed to vary between stroke and intact hemispheres. Standard errors and *P*-values result from non-linear mixed-effects regressions fit either jointly ('joint model') or separately for stroke ('ipsilesional') and intact ('contralesional') hemispheres, using the R package nlme. *P*-values of Δ (separate) and Δ_{ipsi} (joint) of less than 0.05 are marked in bold. SE = standard error.

Table 3 Statistical details of effect of lesion volume on global graph measures

		Joint model			Ipsilesional			Contralesional		
		Estimate	SE	P	Estimate	SE	P	Estimate	SE	P
q ₅₀	a	0.473	0.005	6.62e-155	0.471	0.005	8.29e-80	0.473	0.006	1.20e-73
	b	1.054	0.736	0.1536	1.009	0.599	0.0962	1.018	3.004	0.7356
	Δ	-0.002	0.005	0.6575	0.007	0.005	0.1729	-0.002	0.006	0.7662
	Δ _{ipsi}	0.012	0.005	0.0274						
	Δ _{vol}	0.000	0.002	0.8546	-0.009	0.002	0.0002	-0.001	0.003	0.7092
	Δ _{vol:ipsi}	-0.011	0.003	4.90e-05						
Efficiency	a	7.030	0.030	2.16e-231	7.008	0.031	1.14e-111	7.037	0.036	1.36e-106
	b	1.158	0.885	0.1921	1.089	0.787	0.1704	1.093	1.940	0.5749
	Δ	-0.025	0.030	0.4025	0.002	0.028	0.9546	-0.027	0.031	0.3831
	Δ _{ipsi}	0.043	0.028	0.1304						
	Δ _{vol}	0.009	0.014	0.5286	-0.033	0.013	0.0115	-0.003	0.014	0.8566
	Δ _{vol:ipsi}	-0.054	0.014	0.0002						
Modularity	a	0.021	0.001	3.67e-34	0.021	0.001	1.27e-23	0.021	0.002	3.93e-20
	b	0.604	0.293	0.0403	0.996	0.455	0.0315	0.999	0.960	0.3014
	Δ	0.003	0.002	0.0760	0.002	0.001	0.2207	0.002	0.002	0.1785
	Δ _{ipsi}	-0.002	0.002	0.2850						
	Δ _{vol}	0.000	0.001	0.7787	0.002	0.001	0.0038	0.001	0.001	0.4957
	Δ _{vol:ipsi}	0.002	0.001	0.0058						

Point estimates, standard errors and *P*-values of model parameters obtained from fitting the exponential model (1) to temporal profiles of global graph measures. In the joint model, total change Δ is modelled as a linear function of log lesion volume, with both intercept and slope allowed to vary between stroke and intact hemispheres. Standard errors and *P*-values result from non-linear mixed-effects regressions fit either jointly ('joint model') or separately for stroke ('ipsilesional') and intact ('contralesional') hemispheres, using the R package nlme. *P*-values of Δ_{vol} (separate) and Δ_{vol:ipsi} (joint) of less than 0.05 are marked in bold. q₅₀ = median connectivity; SE = standard error.

Association of network properties with clinical variables

Table 4 reports statistical details of regression analyses between change in global network topology and clinical outcome, adjusted for stroke lesion volume. Greater decline of ipsilesional median connectivity until 1, 3 and 12 months after stroke was associated with higher NIHSS score ($P=0.0354$), lower relative grip strength ($P=0.0218$), and lower FM score ($P=0.0069$) at these time points. Similarly, decrease of global efficiency and increase of global modularity in stroke hemispheres were associated with higher NIHSS scores ($P_{\text{Eff}} = 0.0100$, $P_{\text{Mod}} = 0.0044$) as well as lower relative grip strengths ($P_{\text{Eff}} = 0.0485$, $P_{\text{Mod}} = 0.1585$) and lower FM scores ($P_{\text{Eff}} = 0.0504$, $P_{\text{Mod}} = 0.0303$).

Exploratory *post hoc* tests for associations between change in topology and clinical outcome at fixed time points revealed consistent effects that were strongest after 3 months, but did not, individually, reach statistical significance. Supplementary Figs 7 and 8 provide a visual representation of clinical outcome parameters in relation to change in global network metrics. Stronger associations were observed if lesion volume was not included as a nuisance regressor (Supplementary Table 8). In contrast to change in network topology, absolute values of global graph parameters were not associated with clinical outcome (Supplementary Fig. 9). Global network measures at baseline did not predict clinical parameters at later times.

Mass-univariate two-stage linear and quasi-Poisson regressions identified associations between change in local

connectivity and clinical outcome in a total of seven brain areas. Higher residual NIHSS scores were most strongly associated with loss of local connectivity in pre-central, post-central, inferior frontal and cingulate cortices, as well as the thalamus. Statistical details including lesion volume corrected regression results are provided in Supplementary Tables 9 and 10.

Discussion

Our longitudinal study examined how global network properties of structural brain networks change after ischaemic stroke and how topological variations relate to lesion volume and clinical outcome. We found that structural brain networks after motor stroke evolve over time in both ipsi- and contralesional hemispheres with a drift towards structural degeneration, impaired integration and greater segregation, which was more pronounced in hemispheres directly affected by stroke. In ipsilesional, but not contralesional hemispheres, this change was modulated by the volume of the ischaemic lesion with greater differences in network properties between chronic and acute phases observed in patients with larger strokes. Finally, the magnitude of post-stroke change in structural connectivity was associated with residual symptom burden and motor impairment; for most associations, this was independent of lesion volume. There was no evidence of significant increases in structural integrity of brain networks after stroke.

Brain network disruptions after ischaemic stroke are mediated by loss of structural integrity in white matter

Table 4 Statistical details (corrected for lesion volume) of association between change in global network topology and clinical outcome

		Pooled model			1 month			3 months			12 months		
		Estimate	SE	P	Estimate	SE	P	Estimate	SE	P	Estimate	SE	P
NIHSS	q ₅₀	-21.681	10.113	0.0354	-4.808	12.142	0.6956	-20.699	13.938	0.1517	-13.199	12.755	0.3120
	Efficiency	-5.140	1.944	0.0100	-1.254	2.359	0.5998	-4.160	2.492	0.1092	-2.597	2.172	0.2446
	Modularity	178.002	60.607	0.0044	11.984	61.468	0.8471	157.379	58.341	0.0132	44.011	52.645	0.4121
rGS	q ₅₀	6.236	2.654	0.0218	3.535	3.433	0.3139	3.172	4.091	0.4472	3.240	2.823	0.2654
	Efficiency	1.179	0.587	0.0485	1.065	0.727	0.1567	0.454	0.785	0.5691	0.436	0.516	0.4094
	Modularity	-29.932	20.989	0.1585	1.017	20.549	0.9610	-9.405	24.304	0.7028	-12.808	14.035	0.3729
FM ^a	q ₅₀	-36.726	13.215	0.0069	-17.404	15.792	0.2814	-19.105	18.981	0.3251	-26.294	16.528	0.1259
	Efficiency	-5.192	2.610	0.0504	-2.291	2.722	0.4083	-2.622	3.609	0.4751	-3.089	2.841	0.2886
	Modularity	180.020	81.492	0.0303	-4.026	70.267	0.9548	105.828	90.111	0.2528	91.112	60.574	0.1468

Regression coefficients (point estimates, standard errors and *P*-values) on the link scale between change in global network measures and clinical outcome. Log-transformed lesion volume is included as a nuisance regressor. In the case of NIHSS and FM^a=66-FM scores, quasi-Poisson regressions with a log-link are used; in the case of relative grip strength, a Gaussian regression with identity link is used. The first three columns ('pooled model') represent pooled estimates from joint two-stage regressions across the subacute and chronic stages. *P*-values 0.05 are marked in bold.

FM = Fugl-Meyer; NIHSS = National Institutes of Health Stroke Scale; rGS = relative grips strength; SE = standard error.

tracts. In this study, this was reflected by a decline of numerical connectivity in stroke hemispheres, which occurred predominantly over the first 3 months after the insult. In agreement with previous results on network changes in chronic stroke patients obtained in our group (Cheng *et al.*, 2019b), this ipsilesional network disruption manifested topologically as a decline of global efficiency and an increase in global modularity which were robustly identified in supplementary sensitivity analyses at different network densities. The chosen graph-theoretical measures represent the notions of integration and functional segregation in large-scale networks and are known to be altered in a variety of neurological disorders (Bassett and Bullmore, 2009).

Lesion volume is a known predictor of clinical severity and symptom burden in both the acute and chronic phase of stroke. However, association of infarct volume with clinical outcome and brain function is limited as shown by overall moderate correlations (Shelton and Reding, 2001; Page *et al.*, 2013). In our group of patients with upper extremity motor deficits, size of the ischaemic lesion modulated the extent of topological network changes after stroke in a time-dependent pattern. Larger lesion volumes were associated with both loss of global efficiency and gain in modularity during the subacute and chronic stages, whereas the association between lesion volume and connectome changes at the acute phase 3–5 days after stroke was less pronounced (Fig. 3). We hypothesize that this is due to the relatively small lesion volumes observed in our group of patients, where strategically located lesions [such as the internal capsule, (see Supplementary Fig. 2)] resulted in relevant motor deficits, however, causing only subtle changes in global connectivity or topology of the large-scale structural connectome. During the later time points after stroke, disruptions of the structural brain networks became more apparent and dependent on lesion volume, potentially reflecting the pathophysiological processes of secondary neurodegeneration

known to occur after isolated stroke lesions (Zhang *et al.*, 2012).

In this study, we focused on patients with upper extremity motor deficits as a common and highly relevant clinical impairment in ischaemic stroke. Symptom severity was measured by the NIHSS score, motor impairment by the FM score and relative grip strength, respectively. In our group of patients, we observed a comparatively large between-subject variability of global network metrics and alterations in ipsilesional structural topology which first appeared during the early subacute phase and persisted throughout the chronic phase. We, therefore, hypothesized that the dynamic change of network parameters might be more important for motor outcome than their absolute values at each time point. We found that throughout the study period a greater decline of global efficiency and greater increase in modularity were associated with greater residual symptom burden and motor impairment. The association persisted after correcting for the effect of lesion volume, thus establishing change in global network topology as an important factor for clinical outcome beyond the volume of initially damaged brain tissue.

In general, longitudinal studies of white matter integrity after stroke are far scarcer than reports from cross-sectional investigations. The time course and dynamics of topological network changes in our study are, however, in line with previous studies demonstrating progressive losses of structural integrity in white matter tracts over the period of 3 months after stroke (Koch *et al.*, 2016). Beyond changes of brain structure, reorganization after stroke of functional brain networks involved in motor execution is associated with clinical recovery (Wang *et al.*, 2010). Adaptive changes in functional brain networks might, therefore, account for dynamics of clinical recovery of our patients unexplained by structural network topology. Future work is necessary to elucidate interactions between changes in structural and functional

brain networks after stroke. Despite having long-range global effects on cerebral network architecture, stroke lesions do not equally affect all parts of the structural connectome. Given the selection of patients based on motor deficits of the upper extremities, we expected a distinct pattern of localized changes in network parameters. Using the local graph parameters strength, efficiency and clustering, we localized alterations in topology to brain regions in the frontal, parietal and temporal lobes, as well as subcortical structures (see [Supplementary materials](#)). While some of these regions were affected directly by the ischaemic lesion and are thus expected to display altered connectivity patterns, others reflect the secondary effects of structural disconnections. Our investigation of the association between change in local network topology and clinical outcome identified a sub-network consisting of seven cortical areas including primary motor and premotor, as well as supplementary motor and association cortices involved in planning and execution of motor functions. While motor recovery after stroke in relation to changes in functional brain connectivity has been investigated extensively ([Grefkes and Fink, 2011, 2014](#); [Siegel et al., 2018](#)), reports on changes of large-scale connectivity and topology of structural brain networks after stroke are scarce ([Carter et al., 2012](#); [Aerts et al., 2016](#)). It is, however, known that localized structural lesions induce changes in distant, yet connected brain regions after stroke leading to widespread disruption of white and grey matter integrity. Work from our group demonstrated preferential reduction of cortical thickness in distant brain areas connected to subcortical ischaemic lesions over a time frame of 1 year after stroke ([Cheng et al., 2019a](#)). Changes of local 'connectedness' in cortical brain regions induced by an ischaemic lesion was shown to predict subsequent volumetric atrophy of that area after 6 months ([Kuceyeski et al., 2014](#)). Furthermore, structural connectivity of selected pathways such as the corticospinal tract, alternate corticofugal pathways and selected cortico-cortical connections have been analysed in relation to residual motor function in cross-sectional and longitudinal studies ([Koch et al., 2016](#)).

In terms of large-scale network changes during the early chronic stage after stroke, the effect of focal ischaemic lesions on neurological deficits has been related to changes in the topological properties of the structural brain network in a limited number of cross-sectional studies. Animal studies with experimental stroke models and high-resolution diffusion-tensor MRI demonstrated impaired integration and increased segregation parameters as well as hub shifts of empirical and simulated structural networks ([Sinke et al., 2018](#); [Straathof et al., 2019](#)). In humans, severity of aphasia has been linked to disruption of structural hubs in a language network ([Gleichgerrcht et al., 2015b](#)), apathy and post-stroke depression have been found to be related to reduced local and global efficiency in distributed sub-networks. Structurally, reduced centrality measures in stroke hemispheres ([Lee et al.,](#)

[2015](#)), as well as reduced communicability ([Crofts et al., 2011](#)) and a modified backbone structure in contralateral hemispheres have been described. In a different cohort, nodal centrality measures of the inferior parietal lobe and the posterior cingulate gyrus were associated with motor impairment on the FM scale and immediate recall, respectively ([Zhang et al., 2017](#)). Taken together, these results indicate a common tendency and topological pattern of disintegration in structural brain networks after stroke characterized by an impaired potential of long-range integration of information transfer combined with increased segregation in a more modular network architecture. Our findings are in line with these observations and add novel information concerning the longitudinal evolution of large-scale structural changes in the structural connectome after stroke.

In our study, we found no evidence of specific increases in structural connectivity as a correlate of compensatory brain plasticity. Previous studies indicated co-localized increases of cortical thickness with functional brain activity associated with the recovery of somatosensory deficits after stroke ([Schaechter et al., 2006](#)). Regarding the structural connectome, changes of network measures such as increased communicability have been found in two previous studies and discussed to indicate structural plasticity after stroke ([Crofts et al., 2011](#); [Sinke et al., 2018](#)). In our group of patients, recovery was generally favourable and associated with lower extent of structural disintegration, both in terms of network connectivity and topology. Further studies including data from functional imaging are needed to elucidate the mechanisms of changes in structural connectivity to promote or restrict motor recovery after stroke. Whereas the longitudinal design and detailed clinical and imaging characterization of our patients are strengths of these studies, there are several limitations to consider. Our study design did not include longitudinal structural network data for a group of matched control subjects, which would allow the disentangling of network changes due to ageing from lesion-induced disruptions. However, the relatively short observation period of 1 year, the small effect of age on network topology in healthy individuals ([Caeyenberghs and Leemans, 2014](#); [Zhao et al., 2015](#)), and the characteristic non-linear shape of connectivity changes in our study would speak against ageing-related effects as confounding factors in our study. In our prospective cohort design, subjects were included after the occurrence of stroke. We, therefore, did not have access to detailed pre-stroke imaging or clinical data, prohibiting any conclusions about topological features affecting resilience and vulnerability of networks to focal lesions. Specifically, future studies will have to elicit the interplay between the effect of focal stroke lesions and (pre-existing) white matter alterations and structural network changes after stroke. Our approach to reconstructing the structural connectome using probabilistic tractography is well-established and validated against ground-truth models ([Gao](#)

et al., 2013). Nonetheless, no definite consensus has so far been reached in the community about the optimal choice of algorithm or tuning parameters for network reconstruction. Patients in our cohort had a comparatively low lesion volume and were selected by the presence of motor symptoms. Our results are, therefore, not directly generalizable to more severely affected patients with higher lesion volumes and different stroke phenotypes. However, larger stroke lesion volumes also pose significant challenges for the analysis of structural connectomes in the ipsilesional hemisphere leading to inaccurate image registration and network parcellations.

Conclusion

In summary, we demonstrate that structural brain networks after ischaemic stroke show a dynamic loss of integration and an increase in segregation by 12 months after stroke, paralleling the time course of clinical recovery. Alterations in global topology over time are more pronounced in ipsilesional hemispheres where they are modulated by lesion volume but are also present contralesionally. Residual symptom burden and motor impairment are associated with the extent of altered network architecture independently of lesion volume. Our results motivate further studies of longitudinal evolutions in the human connectome after stroke, particularly in combination with data from functional brain connectivity.

Supplementary material

Supplementary material is available at *Brain Communications* online.

Funding

This research was supported by the German Research Foundation (DFG) through projects A1, C1 and C2 in the SFB-936 Multi-site Communication in the Brain.

Competing interests

The authors report no competing interests.

References

- Abela E, Missimer J, Wiest R, Federspiel A, Hess C, Sturzenegger M, et al. Lesions to primary sensory and posterior parietal cortices impair recovery from hand paresis after stroke. *PLoS One* 2012; 7: e31275.
- Achard S, Bullmore E. Efficiency and cost of economical brain functional networks. *PLoS Comput Biol* 2007; 3: e17.
- Aerts H, Fias W, Caeyenberghs K, Marinazzo D. Brain networks under attack: robustness properties and the impact of lesions. *Brain* 2016; 139: 3063–83.
- Ajilore O, Lamar M, Kumar A. Association of brain network efficiency with aging, depression, and cognition. *Am J Geriatr Psychiatry* 2014; 22: 102–10.
- Akaike H. A new look at the statistical model identification. *IEEE Trans Automat Contr* 1974; 19: 716–23.
- Bassett DS, Bullmore ET. Human brain networks in health and disease. *Curr Opin Neurol* 2009; 22: 340–7.
- Behrens TEJ, Berg HJ, Jbabdi S, Rushworth MFS, Woolrich MW. Probabilistic diffusion tractography with multiple fibre orientations: What can we gain? *Neuroimage* 2007; 34: 144–55.
- Bertolero MA, Yeo BTT, D'Esposito M. The modular and integrative functional architecture of the human brain. *Proc Natl Acad Sci USA* 2015; 112: E6798–807.
- Bill F, Foundation MG. Articles global, regional, and national burden of stroke, 1990–2016: a systematic analysis for the Global Burden of Disease Study 2016. *Lancet Neurol* 2019; 4422: 1–20.
- Buchanan CR, Bastin ME, Ritchie SJ, Liewald DC, Madole J, Tucker-Drob EM, et al. The effect of network thresholding and weighting on structural brain networks in the UK Biobank. *bioRxiv* 2019: 649418. doi: 10.1016/j.neuroimage.2019.116443.
- Bullmore E, Sporns O. Complex brain networks: graph theoretical analysis of structural and functional systems. *Nat Rev Neurosci* 2009; 10: 186–98.
- Caeyenberghs K, Leemans A. Hemispheric lateralization of topological organization in structural brain networks. *Hum Brain Mapp* 2014; 35: 4944–57.
- Carrera E, Tononi G. Diaschisis: past, present, future. *Brain* 2014; 137: 2408–22.
- Carter AR, Shulman GL, Corbetta M. Why use a connectivity-based approach to study stroke and recovery of function? *Neuroimage* 2012; 62: 2271–80.
- Cheng B, Braass H, Ganos C, Treszl A, Biermann-Ruben K, Hummel FC, et al. Altered intrahemispheric structural connectivity in Gilles de la Tourette syndrome. *NeuroImage Clin* 2014a; 4: 174–81.
- Cheng B, Dietzmann P, Schulz R, Boenstrup M, Krawinkel L, Fiehler J, et al. Cortical atrophy and transcallosal diaschisis following isolated subcortical stroke. *J Cereb Blood Flow Metab* 2019a; 0271678X1983158.
- Cheng B, Forkert ND, Zavaglia M, Hilgetag CC, Golsari A, Siemonsen S, et al. Influence of stroke infarct location on functional outcome measured by the modified Rankin scale. *Stroke* 2014b; 45: 1695–702.
- Cheng B, Schlemm E, Schulz R, Boenstrup M, Messé A, Hilgetag C, et al. Altered topology of large-scale structural brain networks in chronic stroke [Internet]. *Brain Commun* 2019b. <https://academic.oup.com/braincomms/advance-article/doi/10.1093/braincomms/fcz020/5581344> (8 October 2019, date last accessed).
- Cheng B, Schulz R, Böenstrup M, Hummel FC, Sedlacik J, Fiehler J, et al. Structural plasticity of remote cortical brain regions is determined by connectivity to the primary lesion in subcortical stroke. *J Cereb Blood Flow Metab* 2015; 35: 1507–14.
- Civier O, Smith RE, Yeh CH, Connelly A, Calamante F. Is removal of weak connections necessary for graph-theoretical analysis of dense weighted structural connectomes from diffusion MRI? *Neuroimage* 2019; 194: 68–81.
- Crofts JJJ, Higham DJJ, Bosnell R, Jbabdi S, Matthews PMM, Behrens T, et al. Network analysis detects changes in the contralesional hemisphere following stroke. *Neuroimage* 2011; 54: 161–9.
- Desikan RS, Ségonne F, Fischl B, Quinn BT, Dickerson BC, Blacker D, et al. An automated labeling system for subdividing the human cerebral cortex on MRI scans into gyral based regions of interest. *Neuroimage* 2006; 31: 968–80.
- Fornito A, Bullmore ET. Connectomics: a new paradigm for understanding brain disease. *Eur Neuropsychopharmacol* 2015; 25: 733–48.

- Fornito A, Zalesky A, Pantelis C, Bullmore ET. Schizophrenia, neuroimaging and connectomics. *Neuroimage* 2012; 62: 2296–314.
- Fugl-Meyer AR, Jääskö L, Leyman I, Olsson S, Steglind S. The post-stroke hemiplegic patient. 1. A method for evaluation of physical performance. *Scand J Rehabil Med* 1975; 7: 13–31.
- Gao Y, Choe AS, Stepniewska I, Li X, Avison MJ, Anderson AW. Validation of DTI tractography-based measures of primary motor area connectivity in the squirrel monkey brain. *PLoS One* 2013; 8: e75065.
- Gleichgerrcht E, Kocher M, Bonilha L. Connectomics and graph theory analyses: novel insights into network abnormalities in epilepsy. *Epilepsia* 2015a; 56: 1660–8.
- Gleichgerrcht E, Kocher M, Nesland T, Rorden C, Fridriksson J, Bonilha L. Preservation of structural brain network hubs is associated with less severe post-stroke aphasia. *Restor Neurol Neurosci* 2015b; 34: 19–28.
- Grefkes C, Fink GR. Reorganization of cerebral networks after stroke: new insights from neuroimaging with connectivity approaches. *Brain* 2011; 134: 1264–76.
- Grefkes C, Fink GR. Connectivity-based approaches in stroke and recovery of function. *Lancet Neurol* 2014; 13: 206–16.
- Griffa A, Baumann PS, Thiran J-P, Hagmann P. Structural connectomics in brain diseases. *Neuroimage* 2013; 80: 515–26.
- Hagmann P, Cammoun L, Gigandet X, Meuli R, Honey CJ, Wedeen VJ, et al. Mapping the structural core of human cerebral cortex. *PLoS Biol* 2008; 6: e159.
- Hendricks HT, van Limbeek J, Geurts AC, Zwarts MJ. Motor recovery after stroke: a systematic review of the literature. *Arch Phys Med Rehabil* 2002; 83: 1629–37.
- Hilgetag C-C, Burns GAPC, O'Neill MA, Scannell JW, Young MP. Anatomical connectivity defines the organization of clusters of cortical areas in the macaque monkey and the cat. *Phil Trans R Soc Lond B* 2000; 355: 91–110.
- Jørgensen HS, Nakayama H, Raaschou HO, Vive-Larsen J, Støier M, Olsen TS. Outcome and time course of recovery in stroke. Part I: outcome. The Copenhagen stroke study. *Arch Phys Med Rehabil* 1995; 76: 399–405.
- Kelly-Hayes M, Wolf PA, Kase CS, Gresham GE, Kannel WB, D'Agostino RB. Time course of functional recovery after stroke: the Framingham study. *Neurorehabil Neural Repair* 1989; 3: 65–70.
- Koch P, Schulz R, Hummel FC. Structural connectivity analyses in motor recovery research after stroke. *Ann Clin Transl Neurol* 2016; 3: 233–44.
- Kuceyeski A, Kamel H, Navi BB, Raj A, Iadecola C. Predicting future brain tissue loss from white matter connectivity disruption in ischemic stroke. *Stroke* 2014; 45: 717–22.
- Kuceyeski A, Monohan E, Morris E, Fujimoto K, Vargas W, Gauthier SA. Baseline biomarkers of connectome disruption and atrophy predict future processing speed in early multiple sclerosis. *NeuroImage Clin* 2018; 19: 417–24.
- Laird NM, Ware JH. Random-effects models for longitudinal data. *Biometrics* 1982; 38: 963–74.
- Lawrence AJ, Chung AW, Morris RG, Markus HS, Barrick TR. Structural network efficiency is associated with cognitive impairment in small-vessel disease. *Neurology* 2014; 83: 304–11.
- Lawrence AJ, Zeestraten EA, Benjamin P, Lambert CP, Morris RG, Barrick TR, et al. Longitudinal decline in structural networks predicts dementia in cerebral small vessel disease. *Neurology* 2018; 90: e1898–910.
- Lee M-H, Shin Y-II, Lee SH, Cha YJ, Kim DY, Han BS. Diffusion tensor imaging to determine the potential motor network connectivity between the involved and non-involved hemispheres in stroke. *Biomed Mater Eng* 2015; 26: S1447–53.
- Lemkaddem A, Daducci A, Kunz N, Lazeyras F, Seeck M, Thiran JP, et al. Connectivity and tissue microstructural alterations in right and left temporal lobe epilepsy revealed by diffusion spectrum imaging. *NeuroImage Clin* 2014; 5: 349–58.
- Lim J-S, Kang D-W. Stroke connectome and its implications for cognitive and behavioral sequela of stroke. *J Stroke* 2015; 17: 256–67.
- Liu J, Zhao L, Li G, Xiong S, Nan J, Li J, et al. Hierarchical alteration of brain structural and functional networks in female migraine sufferers. *PLoS One* 2012; 7: e51250.
- Lyden P. Using the National Institutes of Health Stroke Scale. *Stroke* 2017; 48: 513–9.
- Nakayama H, Stig Jørgensen H, Otto Raaschou H, Skyhøj Olsen T. Recovery of upper extremity function in stroke patients: the Copenhagen stroke study. *Arch Phys Med Rehabil* 1994; 75: 394–8.
- Page SJ, Gauthier LV, White S. Size doesn't matter: cortical stroke lesion volume is not associated with upper extremity motor impairment and function in mild, chronic hemiparesis. *Arch Phys Med Rehabil* 2013; 94: 817–21.
- Pinheiro J, Bates D, DebRoy S. nlme: linear and nonlinear mixed effects models [Internet]. <https://cran.r-project.org/package=nlme> (10 May 2019, date last accessed).
- R Core Team. R: A language and environment for statistical computing. Vienna, Austria: R Foundation for Statistical Computing; 2019.
- Rizopoulos D. Joint models for longitudinal and time-to-event data: with applications in R [Internet]. Chapman and Hall/CRC; 2012. <https://www.taylorfrancis.com/books/9781439872871> (18 June 2019; date last accessed).
- Rubinov M, Sporns O. Complex network measures of brain connectivity: uses and interpretations. *Neuroimage* 2010; 52: 1059–69.
- Sayers A, Heron J, Smith A, Macdonald-Wallis C, Gilthorpe MS, Steele F, et al. Joint modelling compared with two stage methods for analysing longitudinal data and prospective outcomes: a simulation study of childhood growth and BP. *Stat Methods Med Res* 2017; 26: 437–52.
- Schaechter JD, Fricker ZP, Perdue KL, Helmer KG, Vangel MG, Greve DN, et al. Microstructural status of ipsilesional and contralesional corticospinal tract correlates with motor skill in chronic stroke patients. *Hum Brain Mapp* 2009; 30: 3461–74.
- Schaechter JD, Moore CI, Connell BD, Rosen BR, Dijkhuizen RM. Structural and functional plasticity in the somatosensory cortex of chronic stroke patients. *Brain* 2006; 129: 2722–33.
- Schlemm E, Cheng B, Fischer F, Hilgetag C, Gerloff C, Thomalla G. Altered topology of structural brain networks in patients with Gilles de la Tourette syndrome. *Sci Rep* 2017; 7: 10606.
- Schulz R, Koch P, Zimerman M, Wessel M, Bönstrup M, Thomalla G, et al. Parietofrontal motor pathways and their association with motor function after stroke. *Brain* 2015; 138: 1949–60.
- Schulz R, Park E, Lee J, Chang WH, Lee A, Kim YH, et al. Interactions between the corticospinal tract and premotor-motor pathways for residual motor output after stroke. *Stroke* 2017; 48: 2805–11.
- Seitz RJ, Azari NP, Knorr U, Binkofski F, Herzog H, Freund HJ. The role of diaschisis in stroke recovery. *Stroke* 1999; 30: 1844–50.
- Shelton F, Reding MJ. Effect of lesion location on upper limb motor recovery after stroke. *Stroke* 2001; 32: 107–12.
- Siegel JS, Ramsey LE, Snyder AZ, Metcalf NV, Chacko RV, Weinberger K, et al. Disruptions of network connectivity predict impairment in multiple behavioral domains after stroke. *Proc Natl Acad Sci USA* 2016; 113: E4367–76.
- Siegel JS, Seitzman BA, Ramsey LE, Ortega M, Gordon EM, Dosenbach NUF, et al. Re-emergence of modular brain networks in stroke recovery. *Cortex* 2018; 101: 44–59.
- Singh MK, Kesler SR, Hadi Hosseini SM, Kelley RG, Amatya D, Hamilton JP, et al. Anomalous gray matter structural networks in major depressive disorder. *Biol Psychiatry* 2013; 74: 777–85.
- Sinke M, Otte WM, van Meer M, van der Toorn A, Dijkhuizen RM. Modified structural network backbone in the contralesional hemisphere chronically after stroke in rat brain. *J Cereb Blood Flow Metab* 2018; 38: 1642–53.
- Sporns O. The human connectome: origins and challenges. *Neuroimage* 2013; 80: 53–61.
- Sporns O, Honey CJ. Small worlds inside big brains. *Proc Natl Acad Sci USA* 2006; 103: 19219–20.

- Straathof M, Sinke MRT, van der Toorn A, Weerheim PL, Otte WM, Dijkhuizen RM. Differences in structural and functional networks between young adult and aged rat brains before and after stroke lesion simulations. *Neurobiol Dis* 2019; 126: 23–35.
- The MathWorks. MATLAB version 9.2.0.556344. Natick, MA: The MathWorks Inc.; 2017.
- Tuladhar AM, Van Uden IWM, Rutten-Jacobs LCA, Lawrence A, Van Der Holst H, Van Norden A, et al. Structural network efficiency predicts conversion to dementia. *Neurology* 2016; 86: 1112–9.
- Van Den Heuvel MP, Fornito A. Brain networks in schizophrenia. *Neuropsychol Rev* 2014; 24: 32–48.
- Ver Hoef JM, Boveng PL. Quasi-Poisson vs. negative binomial regression: how should we model overdispersed count data? *Ecology* 2007; 88: 2766–72.
- Verheyden G, Nieuwboer A, De Wit L, Thijs V, Dobbelaere J, Devos H, et al. Time course of trunk, arm, leg, and functional recovery after ischemic stroke. *Neurorehabil Neural Repair* 2008; 22: 173–9.
- Wang L, Yu C, Chen H, Qin W, He Y, Fan F, et al. Dynamic functional reorganization of the motor execution network after stroke. *Brain* 2010; 133: 1224–38.
- Wang LE, Tittgemeyer M, Imperati D, Diekhoff S, Ameli M, Fink GR, et al. Degeneration of corpus callosum and recovery of motor function after stroke: a multimodal magnetic resonance imaging study. *Hum Brain Mapp* 2012; 33: 2941–56.
- Watts DJ, Strogatz SH. Collective dynamics of ‘small-world’ networks. *Nature* 1998; 393: 440–2.
- Xu X, Lau KK, Wong YK, Mak H, Hui ES. The effect of the total small vessel disease burden on the structural brain network. *Sci Rep* 2018; 8: 7442.
- Yang S, Hua P, Shang X, Cui Z, Zhong S, Gong G, et al. Deficiency of brain structural sub-network underlying post-ischaemic stroke apathy. *Eur J Neurol* 2015; 22: 341–7.
- Zhang D, Lin X, Sowers MF. Two-stage functional mixed models for evaluating the effect of longitudinal covariate profiles on a scalar outcome. *Biometrics* 2007; 63: 351–62.
- Zhang J, Zhang Y, Wang L, Sang L, Yang J, Yan R, et al. Disrupted structural and functional connectivity networks in ischemic stroke patients. *Neuroscience* 2017; 364: 212–25.
- Zhang J, Zhang Y, Xing S, Liang Z, Zeng J. Secondary neurodegeneration in remote regions after focal cerebral infarction: a new target for stroke management? *Stroke* 2012; 43: 1700–5.
- Zhao T, Cao M, Niu H, Zuo XN, Evans A, He Y, et al. Age-related changes in the topological organization of the white matter structural connectome across the human lifespan. *Hum Brain Mapp* 2015; 36: 3777–92.